We are IntechOpen, the world's leading publisher of Open Access books Built by scientists, for scientists

4,800
Open access books available

122,000
International authors and editors

135M
Downloads

Our authors are among the

154
Countries delivered to

TOP 1%
most cited scientists

12.2%
Contributors from top 500 universities

WEB OF SCIENCE™

Selection of our books indexed in the Book Citation Index in Web of Science™ Core Collection (BKCI)

Interested in publishing with us?
Contact book.department@intechopen.com

Numbers displayed above are based on latest data collected.
For more information visit www.intechopen.com

Chapter 6

Quality Control of Ionizing Radiation in Radiotherapy

Ernesto Lamanna, Bianco Cataldo, Giulia Marvaso,
Marco D'Andrea and Lidia Strigari

Additional information is available at the end of the chapter

http://dx.doi.org/10.5772/60421

Abstract

This work includes the results of our research on the measurement of the dose delivered by an external beam in radiotherapy. The use of scintillating fibers in high-energy experiments produced rapid and reliable results and allows new dosimeters to be built and extends their use to measure the dose of an external beam of electrons, photons, and hadrons in radiotherapy.The chapter starts from the description of the radiation used in radiotherapy, presents the new approaches and then the tools used to perform the quality control of therapeutic beams, and finally shows the characteristics and differences compared to the traditional quality controls by using our results on the scintillating fibers used as a dosimeter. Some care should be taken into account during the collection and processing of data, for the treatment of some systematic errors in the method. In this chapter, we describe the procedure to be followed.

Keywords: radiotherapy, IMRT, dosimeter, scintillating fibers

1. Introduction

The use of ionizing radiation for the treatment of cancer can be traced back to the discovery of X-rays and radioactive isotopes by WC Roentgen (1895), H. Becquerel (1896), and M. and P. Curie (1898). X-rays have been used in clinical medicine since the early years of the twentieth century [1]. Initially, X-rays used energies required for diagnostic purposes and then higher energies (180–200 kV) of the photons produced by X-ray tubes developed to treat tumors. The ability to treat tumors located in deeper tissues was guaranteed later by the development in

the 1950s of linear accelerators of electrons with energies of 4–20 MeV and the production of intense beams of photons with delivery of higher doses [2]. The most important limitation to their use was the excessive radiation in normal tissue surrounding the tumors. To overcome this, the approach of multifield treatment plans has been developed to guarantee the dose necessary for the tumor, thus reducing the high dose to normal tissues. In the same years, the technology developed to produce accelerators of massive particles allowed therapeutic trials of protons and ions to kill cancer cells to be started [3]. The development of more powerful computers allowed treatment plans to be set up with the assistance of the computer, and from 1984, excellent treatment systems with beams of protons and ions for clinical use were realized. The method of treatment with protons and ions is advantageous for its characteristic of maximum energy transfer near the stopping point of the particle. Using electrons or photons the dose delivered is continuously reduced by increasing its depth. For this reason, hadron beams are preferable for deep tumors. Currently, the systems required for the use of hadrons are expensive, and there are few centers in the world in which they are available [4]. The systems that produce beams of electrons and photons are cheaper and have spread widely in health facilities. They are referred to as "conventional radiotherapy." Research for the improvement of their use has produced an impact on the treatment method by introducing new ways to deliver the dose: the intensity-modulated radiation therapy (IMRT) and the volumetric-modulated arc therapy (VMAT). The new methodologies require more accurate detectors for measuring the dose delivered and for assuring quality controls of the system used, with high spatial and temporal resolutions.

2. Ionizing radiation used in radiotherapy

Radiotherapy, also called radiation therapy (RT), indicates the treatment of cancer and other diseases with ionizing radiation, which are used to deposit energy in tumor cells and directly or indirectly damage the genetic material (DNA) in the individual cells, making it impossible for them to continue to grow.

One type of radiation therapy commonly used is with photons, "packets" of energy, or particles, which, depending on the amount of energy they possess, destroy cancer cells on the surface of an area or penetrate to tissues deeper in the body. The higher the energy of the photon beam, the deeper the distance at which a given dose is delivered into the target tissue.

Linear accelerators are generally adopted in Radiotherapy departments to focus ionizing radiation on a cancer site, and this modality is called external beam radiotherapy (EBR). With modern radiation equipment, the radiation is focused on the target thanks to a multileaf collimator (MLC) and a complex sequence of their movements aimed at delivering conformal dose distribution using static or dynamic position of leaves at different static or dynamic gantry positions.

All the above delivery modalities are potentially associated to an on board imaging device in order to improve the treatment setup reproducibility, thanks to 2D/3D imaging based on kV or MV-based imaging.

In fact, in radiation therapy, a sharply defined dose distribution minimizes the side effects of treatment because only small amounts of radiation travel to the surrounding tissues. Gamma rays are produced spontaneously as certain elements (such as cobalt 60) release radiation as they decompose, or decay and are another form of photons used in radiotherapy. Each element decays at a specific rate and gives off energy in the form of gamma rays and other particles.

Another technique for delivering radiation to cancer cells relies on the possibility of placing radioactive implants directly into a tumor or body cavity and are denoted as brachytherapy, interstitial, or intracavity irradiation. This technique is also called internal radiotherapy, and it is appreciated because it is able to deliver high doses concentrated in a small area, generating a high-dose gradient. Internal radiotherapy is sometimes used for cancers of the tongue, uterus, prostate, and cervix but in some cases is considered an invasive procedure.

Other proposed approaches include intraoperative irradiation, in which a large dose of external radiation is directed on to the tumor or tumor bed during surgery, thanks to conventional use of dedicated mobile linear accelerators. Other investigational techniques include the particle beam radiation therapy based on the acceleration of proton or ions to treat localized cancers. The acceleration of these particles requires very sophisticated machines generating modulated or conformal beams to damage tumor cells. Several of these particles, depending on their energy, could produce damage radiobiologically more efficacious than conventional radiotherapy on both tumor and normal tissues, the latter spared by using very conformal dose distributions.

Other recent radiotherapy modalities are based on radiolabeled antibodies to deliver doses of radiation directly to the cancer site due the presence of tumor-specific antibodies (radioimmunotherapy) or in general radionuclides, which thank to their chemical features or their direct injection in the target tissue/tumor bed can target more precisely. The success of this technique will depend upon both the identification of appropriate radioactive substances and the determination of the safe and effective dose of radiation that can be delivered in this way.

Scientists are also looking for ways to increase the effectiveness of existing radiation therapy techniques, based on investigational drugs including radiosensitizers, which make the tumor cells more likely to be damaged, radioprotectors, which protect normal tissues from the effects of radiation, or anti-angiogenic drug, interfering with the neo-angiogenic process. Hyperthermia, or the use of heat, is also being studied for its effectiveness in sensitizing tissues to radiation.

3. New methodology in radiotherapy

Radiation therapy (RT) is an integrated part of the modern comprehensive cancer management. Radiotherapy has seen continuous technological improvements since the discovery of

X-rays in 1895 [5]. The main focus in radiation therapy has always been to increase the level of precision and accuracy of dose delivery to the tumor target volume while sparing normal tissue. Remarkable progress has been made in this area, which is especially based on the new delivery systems, new imaging modalities, and more powerful computers and software. These include, for external beam radiotherapy (EBR), the development of advanced linear accelerators, with higher energies and better dose characteristics and skin sparing, as well as smaller sources for reduced lateral penumbra, which date back to the 1950s [6]. One of the major advances in radiation oncology in the early 1990s was the application of computer-graphics technology to CT scanning, when 2D RT was largely replaced by 3D RT, based on CT imaging. Furthermore, radiation dosimetry based on 3D conformal therapy has been studied more accurately, and Monte Carlo methodology [7] has been also introduced into the current calculation for patient dosimetry. Based on EBTR approach, in the first few years of this century, the next technical step forward consisted of the great interest generated in another form of conformal treatment planning, that is, intensity-modulated radiation therapy (IMRT). IMRT allowed better conformation around the tumor and surrounding normal tissue, involving the delivery of optimized, nonuniform irradiation beam intensities. A uniform dose distribution can be created around the tumor by either modulating the intensity of the beam during its journey through the linear accelerator or by using multileaf collimators (MLCs). IMRT is now available in many clinical departments and can be delivered by linear accelerators with smaller segments of differing MLC shape, such as in the case of static IMRT, or modulated by continuously moving MLC, such as in the case of dynamic IMRT [8]. Other derived techniques include tomotherapy, which uses a dedicated CT scan unit and is well suited to treat large volumes [9]. This has led to improvements in the therapeutic ratio for several tumor sites, such as head and neck [10], prostate [11], and gynecological cancers [12]. Volumetric-modulated arc therapy (VMAT) is an advanced form of IMRT that can be delivered using conventional linear accelerators with conventional MLC. VMAT can provide highly conformal dose distribution and improve the IMRT delivery efficiency significantly. The basic concept of arc therapy is the delivery of radiation by means of a continuous rotation of the radiation source and allows the patient to be treated from a full 360 beam angle. However, a major advantage over fixed gantry IMRT is the improvement in treatment delivery efficiency, as a result of the reduction in treatment delivery time and the reduction in monitor unit (MU) usage, with subsequent reduction of integral radiation dose to the rest of the body [13, 14]. In the last decade, there has been a very rapid growth in the clinical application of stereotactic radiosurgery (SRS) and stereotactic body radiation therapy (SBRT). Although the first stereotactic devices were designed by Leksell [15] for the treatment of intracranial benign or malignant lesions, and this was the primary indication, technical improvements in SBRT planning have allowed its use for extracranial lesions [16]. Stereotactic treatment requires strict immobilization, advanced image guidance, and sophisticated treatment planning and delivery systems, resulting in highly conformal dose distributions that allow decreases in the size of treatment volumes relative to conventional radiotherapy. This, in turn, allows for delivery of large doses of radiation per fraction and increased biologically effective doses (BED) beyond those possible with conventional treatments.

http://dx.doi.org/10.5772/60421

4. Quality control and dosimetry of the beam

IMRT and VMAT treatments are extremely complex and require patients' specific quality assurance be performed to ensure the dose calculated by treatment planning systems to be the actual dose delivered to the patient at the treatment unit. Guidelines for IMRT commissioning have been published by AAPM Task Group (TG) 119 [17]. The guidelines established test cases to benchmark the overall accuracy of IMRT planning and delivery. The AAPM TG 119 relies on two preliminary tests to evaluate a dose calculating module and four commissioning cases: test prostate, head and neck (H&N), C-shaped target, and multitarget [17].

Typically, IMRT patient-specific QA is performed on a linac using a homogeneous phantom and a dose-measuring device to measure the absolute dose in representative points in the phantom or planar doses. This method requires time on a linac and increases the workload for medical physicist staff. Unfortunately, it is difficult to replicate patient geometries and heterogeneity using a phantom-based QA method.

Treatment plan QA software has been proposed to act as an independent plan evaluation and dosimetry check, thus removing the need to carry out measurements. Unfortunately, this method does not take into account potential failure during delivery that could affect the expected fluence flow map generated by linac.

VMAT [14] is an arc-based IMRT to be delivered on a conventional linac provided of MLC. During arc beam delivery, the dose rate, the speed of the gantry, and the position of the MLC leaves can be adjusted dynamically. RapidArc and SmartArc are examples of VMAT. For most of the commercial planning solutions, no more than two arcs are needed to significantly improve the dose conformity. Rotating the MLC by 45° for VMAT can improve monitor unit efficiency [18].

Generally, VMAT deliver doses faster than IMRT, generating plans with higher or at least equivalent quality, with a very few exceptions. Due to necessary synchronization of both dose rate and gantry motion with MLC movement, it is clear that VMAT involves new and different QA steps relative to conventional IMRT. This should be reflected in acceptance testing (AT), commissioning (COM), and routine QA for VMAT. Finally, VMAT uses fewer monitor units resulting in lower patient total body dose. Plan quality is determined by the number of independent aperture variations generated by a conversion algorithm to produce the calculated fluence maps. Specific controls should be used for this purpose [19].

Testing tools and Devices for VMAT Commissioning include dedicated phantoms, electronic portal imager or films, dedicated programmed MLC files (provided by vendors), and software for analysis. Testing protocols should be based on few parameters, defined method, and appropriate tolerance, supported by documentation or specific QA baselines.

In the Ling et al. paper based on a Varian accelerator for testing, proposed procedures were based on a good knowledge of the use of log files and relatively simple equipment.

In the Bedford et al. paper an Elekta accelerator was used for testing based on complex and expensive equipment [20, 21].

To validate VMAT, the understanding of the limits of planning optimization, gantry rotation, beam blocking, couch rotation, leaf speed, and collimator settings is a prerequisite.

Machine-specific QA should include the following:

- Accuracy of the MLC leaf positions during VMAT delivery
- Ability of the system to vary accurately the dose rate and gantry speed during VMAT delivery
- Ability of the system to vary accurately the MLC leaf speed during VMAT delivery
- Tolerances: baselines from commissioning.

The AAPM TG 142 report represents an update on the TG-40 report, specifying new tests and their tolerance, and added recommendations for not only the new ancillary delivery technologies but also for imaging devices that are part of the linear accelerator. In particular, the imaging devices include X-ray imaging, photon portal imaging, and cone-beam CT.

Deviation from the baseline values could result in suboptimal treatment of patients. Machine parameters can deviate from their baseline values as a result of many reasons, such as unexpected changes in machine performance due to machine malfunctioning, mechanical breakdowns, physical accidents, or component failure. Major component replacement (waveguide, bending magnet, etc.) or degradation of components due to the aging of machines may also alter machine performance from the original parameters. These patterns of failure must be considered when establishing a periodic QA program.

Machines used for SRS/SBRT treatments, TBI, VMAT, or IMRT require different tests and/or tolerance. Specific tests could be adopted for dedicated machines such as tomotherapy, VERO, and Cyberknife. For these devices, vendors in some cases provide phantoms and software to be used, such as black box.

The patient-based QA for irradiation techniques involving spatially dishomogenous fluences needs 2D/3D arrays of dosimeters or matrixes (such as Mapcheck/Arccheck, seven-29/Octavius, delta4, MatriXX/Compass, and Gafcromich), EPID-based dosimetric systems (EPIQA, dosimetry check, and DISO) and online systems attached to linac collimator (compass AP and DAVID). To be noted, a dosimetry check has been proposed as useful for tomotherapy, based on measurements from detectors integrated in the accelerators [22–26].

Additional dosimetric issues requiring novel devices/correction factors include the following: (1) small field dosimetry for which ongoing research suggests diamond-based detectors, microchambers, and scintillators; and (2) high-fluence irradiations chambers with appropriate correction factors, alanine, and Gafcromich [27–30].

5. Use of scintillating fibers

Scintillating fibers have been used extensively in experiments of high energy particles. They were used in detector tracers but primarily in calorimetric detectors to measure the corre-

http://dx.doi.org/10.5772/60421

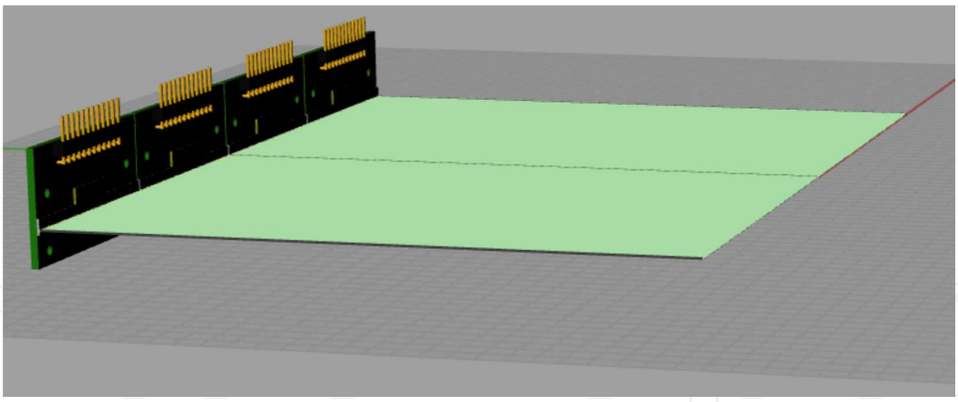

Figure 1. Scintillating fibers, glued in one ribbon, connected to the four arrays of photodiodes.

sponding features of hadronic particles and electromagnetic primaries. The measure of the energy absorbed and the topology of the shower were related to the properties of the incident particle. In recent years, scintillating fibers have been used to measure the density of energy absorbed in the fibers directly and hence the dose delivered by a beam of particles used in radiotherapy. Scintillating fibers have been used in some tests [31–34] in small volumes coupled to light guides for connection to the electronics of conversion and reading; in other tests, they were placed in a water phantom or water equivalent to guarantee an accurate measurement 3D [35–37].

Both the scintillating fibers and the light guides are subjected to the radiation beam in all the tests mentioned. The production of light for Cerenkov effect is negligible in the scintillating fibers compared to the scintillation light [38, 39]; it cannot be ignored in the light guides [40]. Systems with subtraction of this contribution were then required [40].

We experimented a different approach using scintillating fibers, performing tests of therapeutic beams of electrons and photons. The detailed description of the material used and some results have been included in the papers [41–43]. In this chapter, we present the main issues raised and described in previous works and insert recent results obtained using the detector in a vertical configuration.

We used a homogeneous plane of scintillating fibers (380 BCF-60 square scintillating optical fibers produced by Saint Gobain Crystals, each fiber of 0.5 × 0.5 mm^2) directly coupled to the conversion system and reading as shown in Fig. 1.

The fibers are square (0.5 mm per side) and glued in a single ribbon as shown in Fig. 1. To eliminate optical crosstalk among nearby fibers, each fiber is covered with a white EMA (Extra Mural Absorber).

The detector has been made using a ribbon of 20 × 20.5 cm^2 but with a useful sensitive area of 17 × 20.5 cm^2 because 3 cm of the fibers is covered of lead to shield the electronics.

The readout system is composed of photodiodes arranged along four arrays optically coupled with the fiber bundles.

We selected four arrays S8865-128 (Hamamatsu, Shizuoka, Japan), each with 128 photodiodes with a sensitive area of 0.3 × 0.6 mm^2 and a pitch of 0.4 mm assembled as shown in Fig. 1, and four drivers C9118 (Hamamatsu) for the readout in sequence of the photodiodes.

The linear connection between the response in volts and the energy absorbed in the fibers is shown in [41].

The detector was tested using a 6-MV photon beam generated through a Varian Clinac 2100 DHX (Varian Medica Systems, Palo Alto, CA, USA) at the Cosenza Hospital (Cosenza, Italy).

The modalities used for the exposition were the same described by Lamanna et al. [43]. The integration time of 0.3 s was chosen to ensure a dynamic range large enough to have a linear response from the detector.

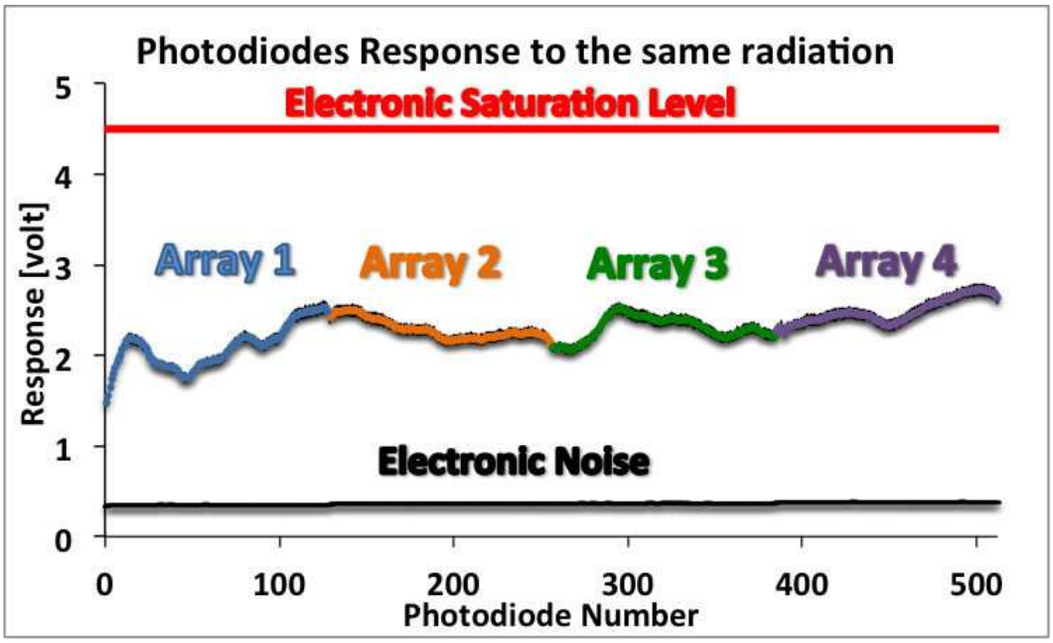

Figure 2. Detector response delivering the same dose to the fibers. The channels of the four arrays of photodiode are shown together with the electronic noise.

The response of the detector to the energy deposited in the scintillating fiber is determined by various contributions such as the production and the propagation of light in the fibers, the electronic gain, the coupling between the fibers and the photodiode array, and geometrical and optical. All these effects have been taken into account measuring a calibration factor for each photodiode response by exposing the fibers to the same dose, as explained in detail by Lamanna et al. [43]. We selected a beam of photons with field of view (FOV) 17 × 28 cm^2, large enough to cover half the size of the ribbon along the fiber axis.

The response of the detector is shown in Fig. 2. The choice of an integration time of 0.3 s ensures a dynamic range wide enough to have a voltage response in the linear region of the electronics readout. This region is limited between the response of the electronic noise and the saturation

voltage. A weight for each channel was estimated to normalize the response of the photodiodes. All the measurements that follow were calibrated using Equation (1):

$$D_i = W_i \times \left(V_i - N_i\right) \text{ with } W_i = \frac{1}{R_i - N_{Ri}} \tag{1}$$

The index i is related to the ith photodiodes. D_i is the relative calibrated response of the photodiode. W_i is the calibration factor (weight). V_i is the measure in volts. N_i is the electronic noise. R_i is the response when all the fibers are exposed to same dose (as shown in Fig. 2). N_{Ri} is the electronic noise associated with the response R_i.

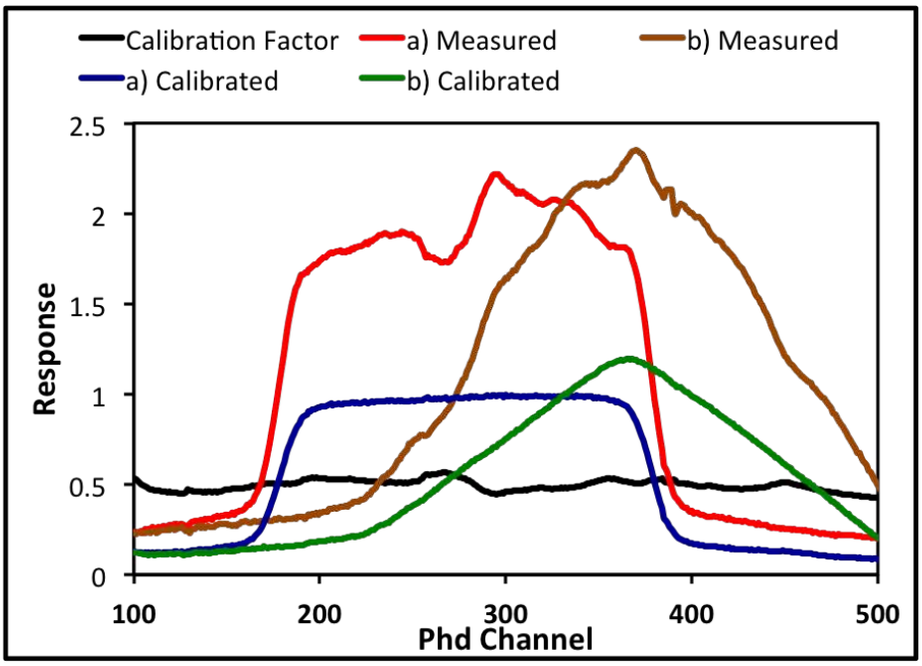

Figure 3. Data taken in two different conditions, (a) red and (b) brown; the same data in blue and green after the calibration.

In Fig. 3, two distributions of data taken in different conditions and the same data after calibration are shown. The procedure described was used for the series of measurements that follow.

6. Dose profile at fixed depth

The dose profile at a fixed depth is reconstructed using an approach very similar to that adopted in X-ray computed tomography [38], reading 1D radon transformation of the dose absorbed.

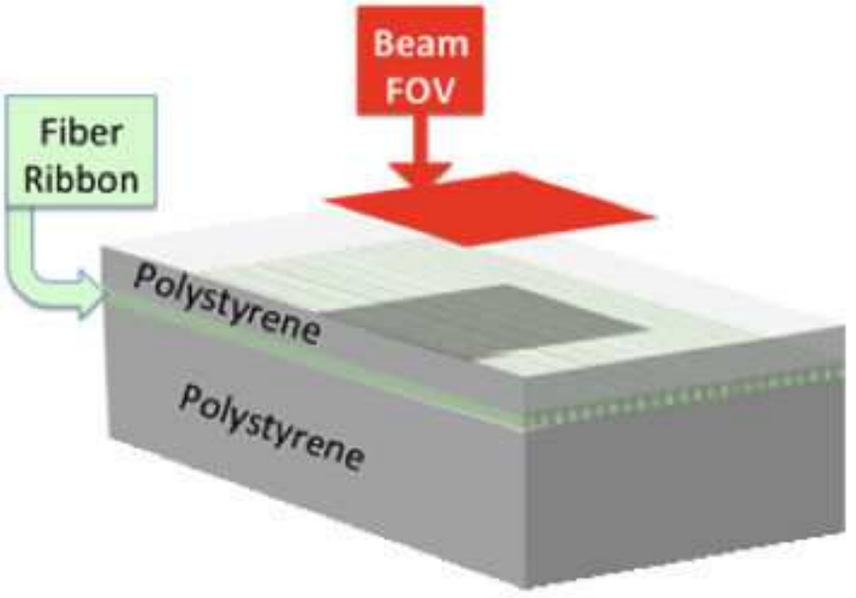

Figure 4. Setup configuration for the horizontal exposition; the red area describes the beam field of view (FOV). The fiber ribbon is enclosed between two sheets of polystyrene to ensure the homogeneity top down.

The response of the detector was tested through exposure to a beam orthogonal to the ribbon surface as shown in Fig. 4. Two passive layers were inserted on the top and bottom of the fibers of thickness, respectively, of 1.6 and 5 cm. The polystyrene of density 1.05 g/cm^3, transparent to the light as the core of the fibers, was selected to build a homogeneous phantom.

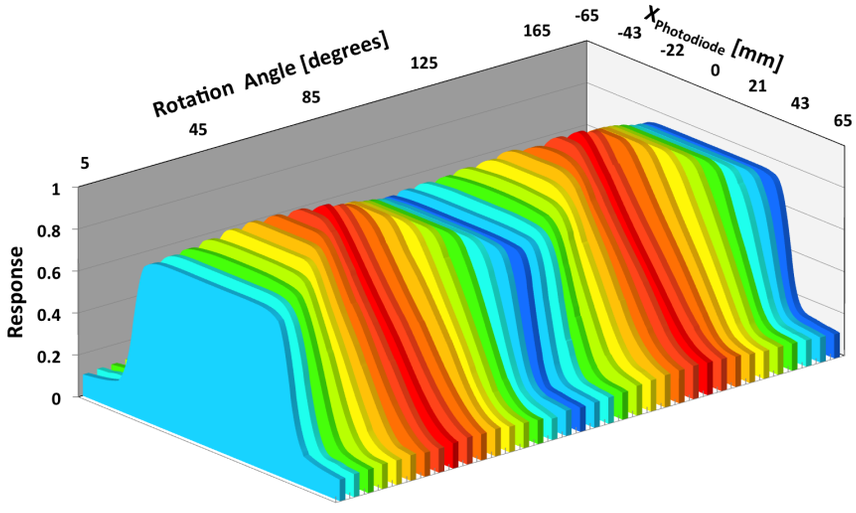

Figure 5. Projected dose at 37 rotating angles around the beam axis. The data are normalized to the maximum value measured.

The field of view (FOV) of 8 × 8 cm^2 was selected. The system was rotated manually around the beam axis, and the data were collected every 5° for a total of 36 positions from 5° to 180°. The distribution of doses, on the axis orthogonal to that of the fibers, is shown for each angle

of rotation in Fig. 5. We observe a variation of the dose and of the width of the distributions, by varying the angle. Angles with maximum dose and minimum width are 45° and 135°, corresponding to a fiber orientation in the direction of the diagonals of rectangular FOV of the beam.

The 36 projections were used to reconstruct the transverse profile of the dose. Using a back-projection approach without filter, we obtained a poor profile, while the reconstruction, shown in Fig. 6, top left, seems to be more precise with the introduction of a ramp filter. A better reconstruction is obtained using the Hann filter, shown in Fig. 6, top right.

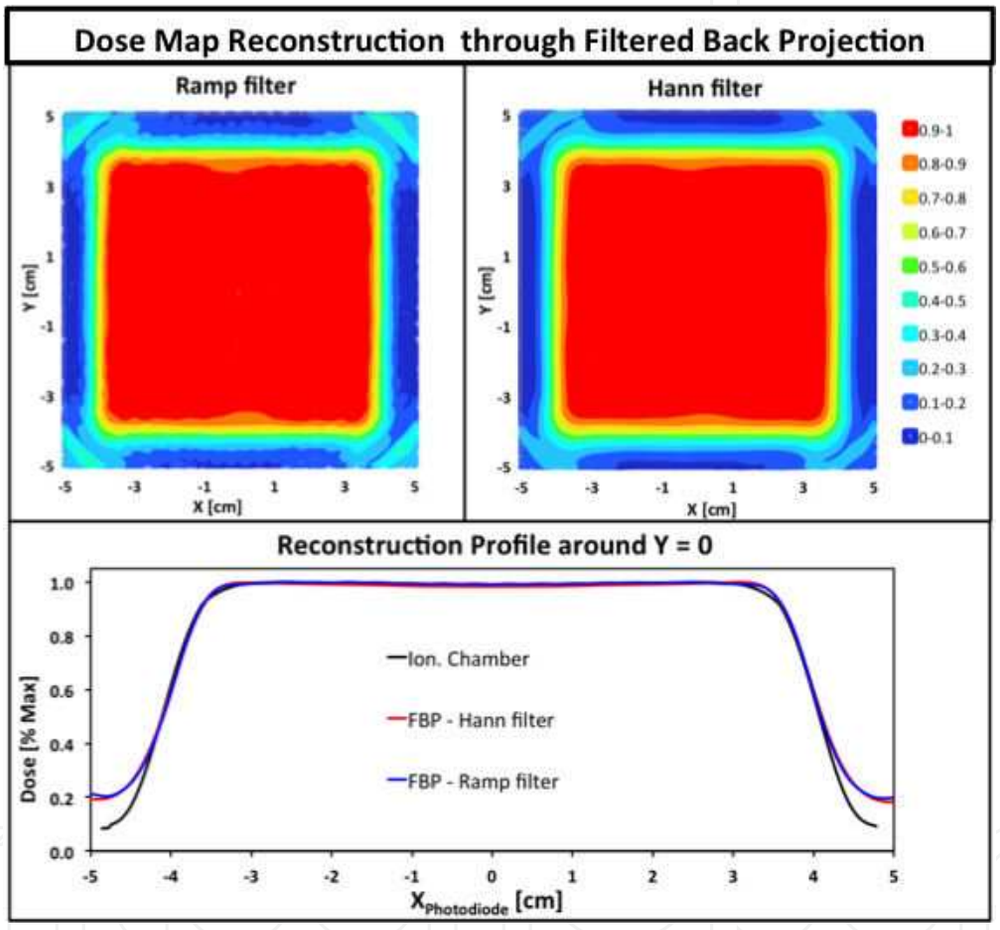

Figure 6. Top: dose map reconstruction using a filtered back projection with ramp filter (left) and Hann filter (right). Bottom: comparison dose profile around $Y = 0$ measured using an ionization chamber superimposed on the reconstructed dose profiles using the back projection with and without filters.

A more accurate comparison is shown at the bottom of Fig. 6 where the reconstructed dose profiles, around the center of the beam, are superimposed on the profile obtained using the PTW Freiburg TM31010 ionization chamber. The reconstruction through the back projection approach with ramp or Hann filter, described in [44, 45], reproduces quite accurately the dose profile. A more detailed description of the method and some comments are provided by Lamanna et al. [43].

7. Percentage depth dose

The delivered dose in depth was measured by rotating the detector in a vertical exposition of the layer, as shown in Fig. 7.

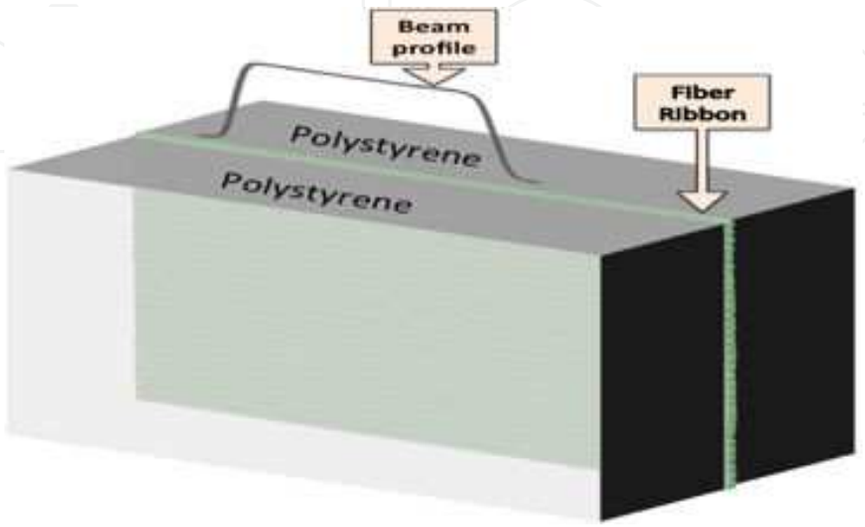

Figure 7. Configuration of the detector for the vertical exposure.

The photon beam was delivered to the sensitive layer placed between two polystyrene sheets of 2.5 cm of thickness. An FOV of 6 × 6 cm^2 was selected to contain the beam completely all along the fiber. In this configuration, the dose is measured along a line in the FOV area and a granularity of 0.5 mm in depth.

The percentage dose in depth (PDD) measured through the fiber detector (b) is superimposed on those obtained using the PTW TM31010 ionization chamber and the water phantom PTW MP3 (PTW, Freiburg, Germany) (a) in Fig. 8. The response of the fibers after the calibration is shown in curve c.

Two features emerge from the comparison of curves a and c:

- Shift of the point of maximum dose
- Different slopes of the curves

The fiber response is in agreement with the ionization chamber after two corrections of the data. The first correction is reported in Equation (2):

$$\begin{gathered} \mathrm{PDD}_i^d = W_i * \mathrm{PDD}_i^c \text{ with } W_i = \frac{\mathrm{width}_0}{\mathrm{width}_i} \\ \mathrm{width}_0 = 6\,\mathrm{cm}\ ; \mathrm{width}_i = 0.08*\mathrm{width}_0 + 6\,cm \end{gathered} \tag{2}$$

http://dx.doi.org/10.5772/60421

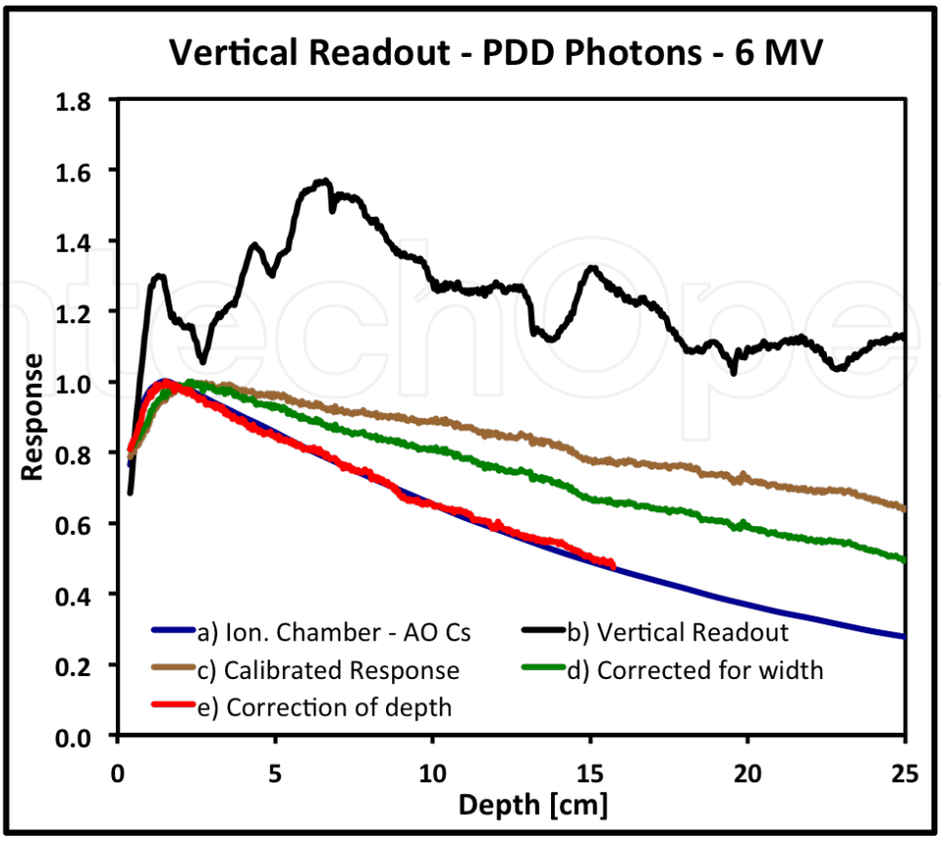

Figure 8. Percent dose depth (PDD) as a function of the depth. The blue curve (a) is the PDD measure through ionization chamber and water phantom at AO Cs; the black points (b) are the measured values in Volt; the brown points (c) are the (b) values, calibrated and normalized to the maximum value; the green points (d) are the (c) values corrected for width; the red points (e) are the (d) values after the correction of the depths.

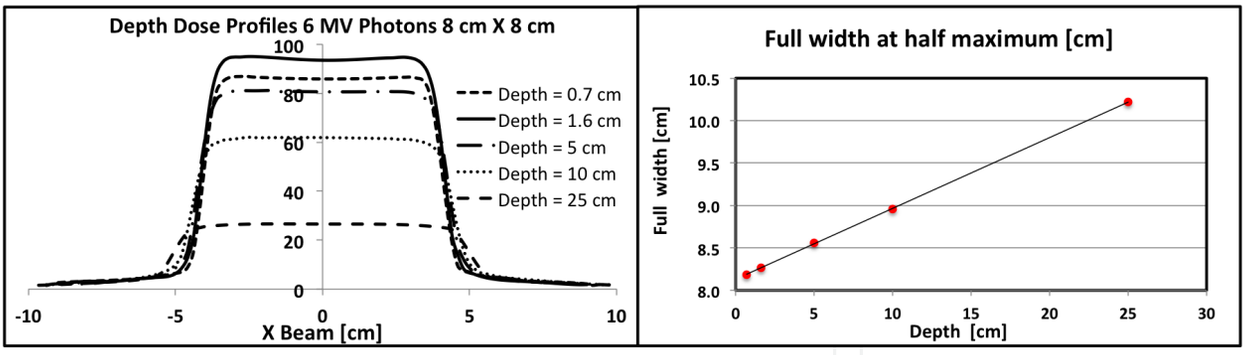

Figure 9. Left side: dose profiles at different depths measured through the ionization chamber and a water phantom in the center of the FOV. Right side: full width at half maximum of the previous profiles as a function of the depth.

The integrated doses along each fiber are measured through the scintillating fibers, and the region of the absorbed dose increases in width as a function of the depths. The behavior is shown in the left region of Fig. 9, where the profiles of the dose at different depth in water for a 6-MV photon beam are plotted. The full width at half maximum of the profiles increases linearly with the depth, as shown on the right of Fig. 9.

The correction factor W_i guarantees the same integration length for all the fibers at different depths. The results are shown in curve d of Fig. 8. The slope is close to that of the curve obtained through the ionization chamber but they are not equal.

The second correction is reported in Equation (3):

$$\text{Depth}_i^{H_2O} = IW_i \times \text{Depth}_i^{C_8H_8} \text{ with } IW_i = \frac{\text{ionization}\left(H_2O\right)_i}{\text{ionization}\left(C_8H_8\right)_i} \tag{3}$$

In the assembled configuration to measure the PDD, shown in Fig. 7, both the layer of scintillating fibers and the passive sheets are mainly made up of transparent polystyrene (C_8H_8). The ionization is different from that in the water at the same depth. The correction factor IW_i is needed to find the depth in water corresponding to the ionization measured in polystyrene.

The factor *IW* has been measured by exposing two phantoms, a water and a transparent polystyrene phantom, in the same conditions. We used a beam of electrons of 9 MeV. The results are shown in Fig. 10. The two behaviors are different. The correction factor in depth IW has been evaluated to produce a full superposition.

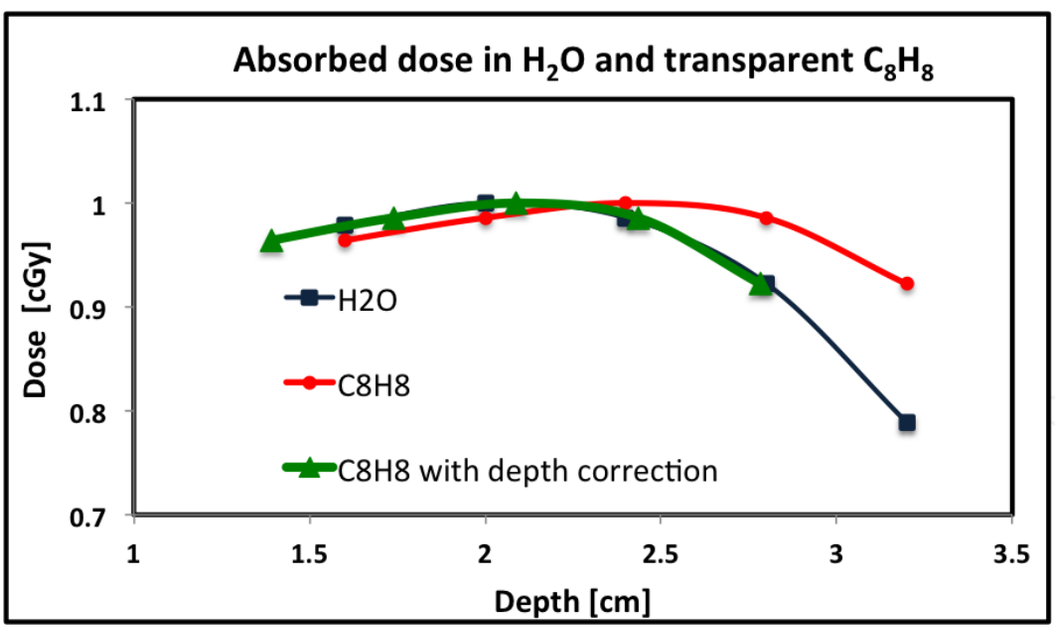

Figure 10. Dose measured through the ionization chamber, in water (black) and in a phantom of transparent polystyrene (red), at different depths. A correction factor for the depth has been evaluated to superimpose the two sets of data. The green points are the red points with the correction of the depths using Equation (3).

The layer of scintillating fibers can be used to measure the PDD in a vertical configuration of the exposure, taking into account that the integration of the dose along the fiber requires the corrections inserted in Equations (2) and (3).

8. Conclusions

The new techniques of delivering the therapeutic dose to the tumor tissues with an external beam require dosimeters that have better spatial and time resolutions than the standard detectors used in current clinical practice. The properties of scintillating fibers of dimensions less than 1 mm and their gluing in homogeneous layers allow these requirements to be obtained. The single-layer 1D can be used to reconstruct the dose profiles XY at a fixed depth, adopting the tomographic technique of filtered back-projection. The same configuration 1D may be used to measure the dose profiles in depth by applying the corrections inserted in Equations (2) and (3).

The final response is quite rapid. The data are acquired in few milliseconds and processed in 2–3 s, using a single layer. This characteristic together with the reduced thickness of two orthogonal layers in a 2D configuration (1 mm of water equivalent), allow the use of layers of fibers also online to measure the characteristics of an incident beam (a similar approach was published in [46]).

The positive results obtained and described in this chapter justify an investment of this approach and suggest some directions for future developments:

a. Acquisition can be speeded up by automating the process of rotation of the dosimeter.

b. The tomographic reconstruction can be improved by introducing iterative reconstruction methods available in the literature.

c. A 3D detector can be achieved by assembling layers 1D orthogonally to the beam axis in a solid phantom.

d. N.B. to realize point c: it is necessary to change the reading system by introducing MPPC or FPD to the arrays of photodiodes.

Nomenclature

AAPM; American Association of Physicists in Medicine

AT ; acceptance testing

COM ; commissioning

EBR; external beam radiotherapy

EBTR; evidence-based timeline retrospective

FOV; field of view

FPD; flat panel detector

IMRT; intensity-modulated radiation therapy

MLC; multileaf collimator

MPPC; multipixel photon counters

PDD; percentage depth dose

QA; quality assurance

SRS; stereotactic radiosurgery

RT; radiotherapy

TBI; traumatic brain injury

UM; monitor units

VMAT; volumetric-modulated arc therapy

Acknowledgements

We are grateful to the Italian INFN (National Institute of Nuclear Physics) for supporting the study of scintillating fiber dosimeters and the "Hospital of Cosenza" for allowing the use of the accelerator Varian to test the dosimeter.

Author details

Ernesto Lamanna[1*], Bianco Cataldo[2], Giulia Marvaso[2], Marco D'Andrea[3] and Lidia Strigari[3]

*Address all correspondence to: lamanna@unicz.it

1 Department of Health Sciences, Magna Graecia University, Catanzaro, Italy

2 Department of Experimental and Clinical Medicine, Magna Graecia University, Catanzaro, Italy

3 Department of Medical Physics, Istituto Regina Elena, Roma, Italy

References

[1] Raju MR. Particle radiotherapy: historical developments and current status. Radiat Res 1996; 145, 391–407.

[2] Slater JM. From X-rays to ion beams: a short history of radiation therapy. In: U. Linz. (Ed.), Ion Beam Therapy. Biological and Medical Physics, Biomedical Engineering. Berlin: Springer-Verlag, 2012. DOI: 10.1007/978-3-642-21414-1 1.

[3] Baskar R, Lee KA, Yeo R, Yeoh. Cancer and radiation therapy: current advances and future directions. Int J Med Sci 2012;9(3):193–9. DOI: 10.7150/ijms.3635. Available from http://www.medsci.org/v09p0193.htm

[4] Thariat J, Hannoun-Levi J-M, Sun Myint A, Vuong T, Gérard J-P. Past, present, and future of radiotherapy for the benefit of patients. Nat Rev Clin Oncol 2013;10, 52–60; published online 27 November 2012. Doi: 10.1038/nrclinonc.2012.203.

[5] Bernier J, Hall EJ, Giaccia A. Radiation oncology: a century of achievements. Nat Rev Cancer. 2004 Sep;4(9):737–47. Review.

[6] Bortfeld T, Jeraj R. The physical basis and future of radiation therapy. Br J Radiol. 2011 Jun;84(1002):485–98.

[7] Spezi E, Lewis G. An overview of Monte Carlo treatment planning for radiotherapy. Radiat Prot Dosimetry 2008;131(1):123–9.

[8] Brahme A. Development of radiation therapy optimization. Acta Oncol 2000;39(5): 579–95. Review.

[9] Goffman TE, Glatstein E. Intensity-modulated radiation therapy. Radiat Res 2002 Jul; 158(1):115–7. Review.

[10] Feng FY, Kim HM, Lyden TH, Haxer MJ, Feng M, Worden FP, Chepeha DB, Eisbruch A. Intensity-modulated radiotherapy of head and neck cancer aiming to reduce dysphagia: early dose–effect relationships for the swallowing structures. Int J Radiat Oncol Phys 2007;68: 1289–98.

[11] Wang-Chesebro A, Xia P, Coleman J, Akazawa C, Roach M 3rd. Intensity-modulated radiotherapy improves lymph node coverage and dose to critical structures compared to with three-dimensional conformal radiation therapy in clinically localized prostate cancer. Int J Radiat Oncol Phys 2006;66: 654–62.

[12] Mundt AJ, Lujan AE, Rotmensch J, Waggoner SE, Yamada SD, Fleming G, Roeske JC. Intensity-modulated whole pelvic radiotherapy in women with gynecologic malignancies. Int J Radiat Oncol Phys 2002;52:1330–7.

[13] Palma DA, Verbakel WF, Otto K, Senan S. New developments in arc radiation therapy: a review. Cancer Treat Rev 2010;36:393–9.

[14] Yu CX, Li XA, Ma L, Chen D, Naqvi S, Shepard D, et al. Clinical implementation of intensity-modulated arc therapy. Int J Radiat Oncol Biol Phys 2002;53:453–63.

[15] Leksell, L. The stereotaxic method and radiosurgery of the brain. Acta Chir Scand 1951;102:316–9.

[16] Salama JK, Kirkpatrick JP, Yin FF. Stereotactic body radiotherapy treatment of extracranial metastases. Nat Rev Clin Oncol 2012;9:654–5.

[17] Ezzell GA, Burmeister JW, Dogan N, et al. IMRT commissioning: multiple institution planning and dosimetry comparisons, a report from AAPM Task Group 119. Med Phys 2009;36(11):5359–73.

[18] Yu CX. Intensity-modulated arc therapy with dynamic multileaf collimation: an alternative to tomotherapy. Phys Med Biol 1995;40:1435–49.

[19] Phillips MH, Holdsworth C. When is better best? A multi-objective perspective. Med Phys 2011;38:1635.

[20] Ling C, et al. Commissioning and quality assurance of RapidArc radiotherapy delivery system. Int J Radiat Oncol Biol Phys 2008;72:575–81.

[21] Bedford JL, Warrington AP. Commissioning of volumetric modulated arc therapy. Int J Radiat Oncol Biol Phys 2009;73:537–45.

[22] Hussein M1, Rowshanfarzad P, Ebert MA, Nisbet A, Clark CH. A comparison of the gamma index analysis in various commercial IMRT/VMAT QA systems. Radiother Oncol 2013 Dec;109(3):370–6.

[23] Watanabe Y, Nakaguchi Y. 3D evaluation of 3DVH program using BANG3 polymer gel dosimeter. Med Phys 2013 Aug;40(8).

[24] Nakaguchi Y, Araki F, Ono T, Tomiyama Y, Maruyama M, Nagasue N, Shimohigashi Y, Kai Y. Validation of a quick three-dimensional dose verification system for pretreatment IMRT QA. Radiol Phys Technol. 2014 Sep 27.

[25] Fredh A, Scherman JB, Fog LS, Munck af Rosenschöld P. Patient QA systems for rotational radiation therapy: a comparative experimental study with intentional errors. Med Phys 2013 Mar;40(3).

[26] Cilla S, Azario L, Greco F, Fidanzio A, Porcelli A, Grusio M, Macchia G, Morganti AG, Meluccio D, Piermattei A. An in-vivo dosimetry procedure for Elekta step and shoot IMRT. Phys Med 2014 Jun;30(4):419–26.

[27] Marsolat F, Tromson D, Tranchant N, Pomorski M, Le Roy M, Donois M, Moignau F, Ostrowsky A, De Carlan L, Bassinet C, Huet C, Derreumaux S, Chea M, Cristina K, Boisserie G, Bergonzo P. A new single crystal diamond dosimeter for small beam: comparison with different commercial active detectors. Phys Med Biol 2013 Nov 7;58(21):7647–60.

[28] Di Venanzio C, Marinelli M, Milani E, Prestopino G, Verona C, Verona-Rinati G, Falco MD, Bagalà P, Santoni R, Pimpinella M. Characterization of a synthetic single crystal diamond Schottky diode for radiotherapy electron beam dosimetry. Med Phys 2013 Feb;40(2).

[29] Podesta M, Nijsten SM, Persoon LC, Scheib SG, Baltes C, Verhaegen F. Time dependent pre-treatment EPID dosimetry for standard and FFF VMAT. Phys Med Biol 2014 Aug 21;59(16):4749–68.

[30] Francescon P, Kilby W, Satariano N. Monte Carlo simulated correction factors for output factor measurement with the CyberKnife system-results for new detectors and correction factor dependence on measurement distance and detector orientation. Phys Med Biol 2014 Mar 21;59(6):N11–7.

[31] Archambault L, Arsenault J, Gingras L, Beddar AS, Roy R, Beaulieu L. Plastic scintillation dosimetry: optimal selection of scintillating fibers and scintillators. Med Phys 2005;32:2271–2278.

[32] Frelin AM, Fontbonne J-M, Ban G, Batalla A, Colin J, Isambert A, Labalme M, Leroux T, Vela A. A new scintillating fiber dosimeter using a single optical fiber and a CCD camera. IEEE Trans Nucl Sci 2006;53 (3):1113–1117.

[33] Lee B, Jang KW, Cho DH, Yoo WJ, Shin SH, Kim H, Yi JH, Kim S, Cho H, Park B, Moon JH, Kim S. Measurement of two-dimensional photon beam distributions using a fiber-optic radiation sensor for small field radiation therapy. IEEE Trans Nucl Sci 2008;55 (5):2632–2636.

[34] Staub D, Cailleret J, Guyonnet JL, Le TD, Wurtz J. Real-time radio-transparent dosimeter for X-ray imaging system. Nucl Instrum Methods Phys Res A 2004;525, 303–307.

[35] Fontbonne JM, Iltis G, Ban G, Battala A, Vernhes JC, Tillier J, Bellaize N, Brun CL, Tamain B, Mercier K, Motin JC. Scintillating fiber dosimeter for radiation therapy accelerator. IEEE Trans Nucl Sci 2002;49 (5):2223–2227.

[36] Guillot M, Gingras L, Archambault L, Beddar S, Beaulieu L. Toward 3D dosimetry of intensity modulated radiation therapy treatments with plastic scintillation detectors. J Phys Conf Ser 2010;250:1–5.

[37] Lacroix F, Beaulieu L, Gingras L, Guillot M. Clinical prototype of a plastic water-equivalent scintillating fiber dosimeter array for QA application. Med Phys 2008;35:3682–3690.

[38] Frelin A-M, Fontbonne J-M, Ban G, Batalla A, Colin J, Isambert A, Labalme M, Vela TLA. A new scintillating fiber dosimeter using a single optical fiber and a CCD camera. IEEE Trans Nucl Sci 2006;53 (3):1113–1117.

[39] Lee B, et al. Characterization of one-dimensional fiber-optic scintillating detectors for electron-beam therapy dosimetry. IEEE Trans Nucl Sci 2008;55 (5):2627–2631.

[40] Archambault L, Gingras L, Beaulieu L, Beddar AS. Measurement accuracy and Cerenkov removal for high performance, high spatial resolution scintillation dosimetry. Med Phys 2006;33,128–135.

[41] Lamanna E, Fiorillo AS, Bruno C, Santaniello A, Siaka YFT, Berdondini A, Bettuzzi M, Brancaccio R, Casali F, Morigi MP, Barca G, Castrovillari F. Dosimetry of high intensity electron beams produced by dedicated accelerators in intra-operative radiation therapy (IORT). IEEE Trans Nucl Sci 2009;56 (1):66–72.

[42] Lamanna E, Fiorillo AS, Gallo A, Trapasso A, Caroleo R, Brancaccio R, Barca G, Carnevale S, Castrovillari F, Tchuente Siaka YF. Dosimetric study of therapeutic beams using a homogeneous scintillating fiber layer. Nuclear Science Symposium and Medical Imaging Conference (NSS/MIC), 2011 IEEE, pp. 244–248, 23–29 Oct. 2011. ISBN: 978-1-4673-0119-0.

[43] Lamanna E, Fiorillo AS, Gallo A, Trapasso A, Caroleo R, Brancaccio R, Barca G, Carnevale S, Castrovillari F, Tchuente Siaka YF. Dosimetric study of therapeutic beams using a homogeneous scintillating fiber layer. IEEE Trans Nucl Sci 2013;60 (1):109–14.

[44] Quinto ET. Tomographic reconstructions from incomplete data-numerical inversion of the exterior Radon transform. Inverse Problems 1988;4 (3):867.

[45] Lyra M, Ploussi A. Filtering in SPECT image reconstruction. Int J Biomed Imaging 2011; ID 693795.

[46] Goulet M, Gingras L, Beaulieu L. Real-time verification of multileaf collimator-driven radiotherapy using a novel optical attenuation-based fluence monitor. Med Phys 2011;38:1459–1459.